Edge selective gas detection using Langmuir films of graphene platelets

Article (Accepted Version)

Surfaces, Interfaces, and Applications

Edge Selective Gas Detection using Langmuir Films of Graphene Platelets

Sebastian Nufer, Matthew J. Large, Alice A. K. King, Sean Paul Ogilvie, Adam Brunton, and Alan B. Dalton

ACS Appl. Mater. Interfaces, **Just Accepted Manuscript** • DOI: 10.1021/acsami.8b05105 • Publication Date (Web): 01 Jun 2018

Edge Selective Gas Detection using Langmuir Films of Graphene Platelets

Sebastian Nufer[a,b,], Matthew J. Large[b], Alice A. K. King[b], Sean P. Ogilvie[b], Adam Brunton[a], and Alan B. Dalton[b,*]*

a M-Solv Ltd, Oxonian Park, Langford Locks, Kidlington, Oxford, OX5 1FP, U.K.

b Department of Physics and Astronomy, University of Sussex, Brighton, BN1 9RH, U.K.

KEYWORDS : graphene, commercial, Langmuir, gas adsorption, electronic doping

ABSTRACT

Recent advances in large-scale production of graphene have led to the availability of solution-processable platelets at the commercial scale. Langmuir-Schaefer (L-S) deposition is a scalable process for forming a percolating film of graphene platelets which can be used for electronic gas sensing. Here, we demonstrate the use of this deposition method to produce functional gas sensors, using a chemiresistor structure from commercially-available graphene dispersions. The sensitivity of the devices and repeatability of the electrical response upon gas exposure has been

characterized. Raman spectroscopy and Kelvin probe force microscopy (KPFM) show doping of the basal plane using ammonia (n-dopant) and acetone (p-dopant). The resistive signal is increased upon exposure to both gases showing that sensing originates from the change in contact resistance between nanosheets. We demonstrate that Arrhenius fitting of the desorption response potentially allows measurements of the desorption process activation energies for gas molecules adsorbed onto the graphene nanosheets.

1.Introduction

Graphene has shown many potential applications in electronic devices such as solar cells and transistor configurations.[1] It has also shown promising results in electrochemical and bio-sensors.[2] Specifically for gas sensing applications[3] promising results have been demonstrated; such as the detection of individual NO_2 molecules in a Hall bar structure,[4] a chemiresistor with an estimated detection limit of 158 ppq (part per quadrillion),[5] or sensor arrays based on reduced graphene oxide which are selective and overcome the problem of device-to-device variations.[6,7] Pristine graphene is known to interact with multiple gases,[8] and chemical functionalization of graphene is used to enable selective detection of different gases.[9] Various device structures to characterise the graphene response to gas exposure have been investigated; among them, chemiresistor structures[10] or the transistor configuration.[11] Rumyantsev et al.[11] were able to distinguish applied gases in the low-frequency noise of pristine graphene when fabricated into a transistor configuration. Graphene has also been incorporated into hybrid structures, such as with silver nanowires, for gas sensing.[12]

Graphene is becoming a commercially available material, with products consisting of small graphene platelets (of the order of 100 nm to 1 μm) that can be purchased in powder form or as dispersions in a variety of solvents or surfactants. Often graphene applications use exfoliated materials or CVD grown sheets which are transferred to a targeted substrate where further photolithography steps are required to fabricate a device.[13] Materials created with these methods are not yet available in industrial quantities, even though simple one step CVD processes have been demonstrated,[14] and photolithography is an expensive method to create electrodes for chemiresistor devices. To make a step towards industrial fabrication of graphene based gas sensors scalable and inexpensive methods of manufacturing electrodes are necessary. Pulsed laser ablation[15] is a fast and efficient method for creating interdigitated electrodes (IDE) which are required for chemiresistive devices. This method requires structuring the electrodes before the deposition of the sensing material and a scalable method for producing percolating thin films from small-platelet graphene dispersions. Langmuir-Schaefer deposition is a method of controllably producing thin material films on electrodes. Percolating graphene films from Langmuir-Schaefer deposition have been shown,[16,17] as well as the sensitivity of such films to hydrogen.[18] Due to the nature of such networks the electrical resistance is dominated by the inter-sheet resistance rather than the basal plane conductivity of the graphene nanosheets.[19] Here we show that Langmuir-Schaefer deposited commercial graphene platelets on laser ablated IDEs can be used to produce gas sensors in which the signal depends on the change in the contact resistance between the nanosheets in the network. KPFM and Raman spectroscopy are used to analyse the doping of the network

and the response of the sensor is characterized using ammonia as an electron donor gas and acetone as an electron acceptor gas.

2.Results and Discussion

Figure 1a and 1b show the manufacturing method of the chemiresistor structure as described in the experimental section.

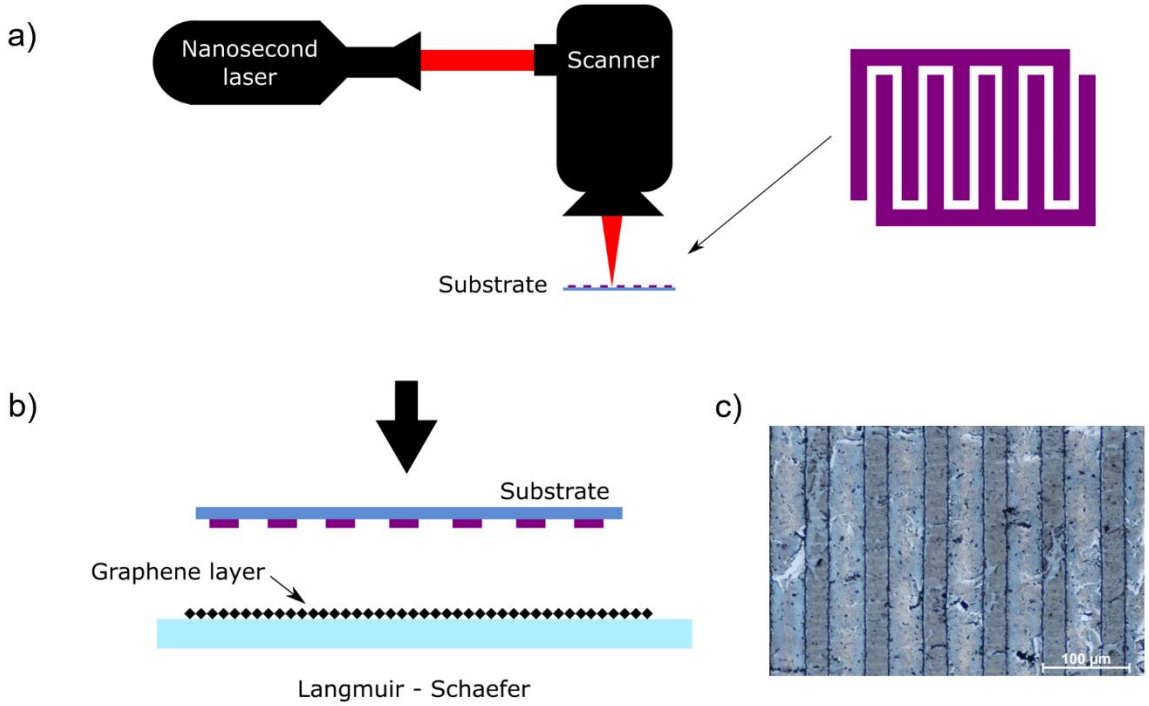

Figure 1 (a) Experimental laser setup used to ablate interdigitated electrodes into a metallic substrate. An infrared nanosecond laser is guided into a Galvoscanner which scribes the designed pattern into the substrate, (b) Langmuir – Schaefer was used to directly deposit graphene on to the IDEs, (c) optical micrograph of the fabricated device

Figure 1c shows an optical micrograph of the fabricated device where the graphene film connects the individual fingers of the IDE structure. The typical response of the sensor when exposed to NH_3 is shown in **Figure 2**. The resistance of the device increases with

increasing concentration of NH_3 but responds repeatably when repeatedly exposed to the same concentration. A drift in the sensor signal is visible which is due to desorption processes which happen over much longer timescales than the measurement cycle time.

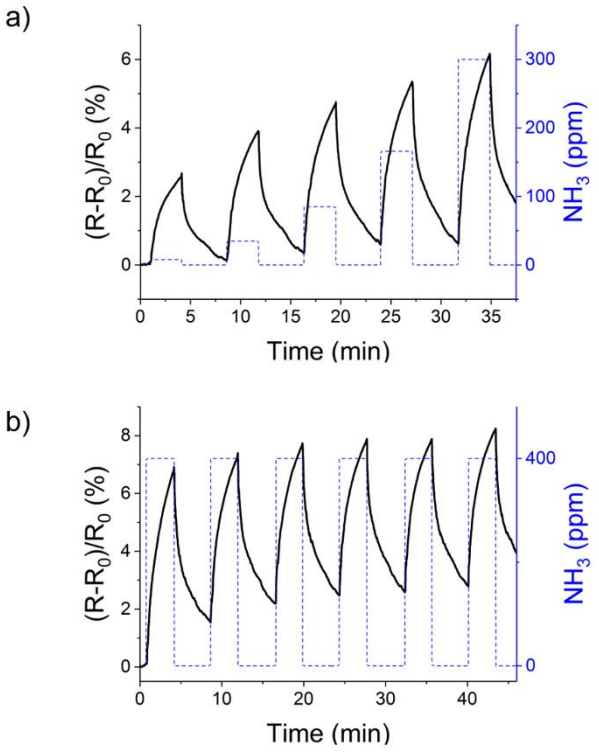

Figure 2 (a) relative signal to various concentrations of NH_3, (b) relative signal to a repeated concentration of 400 ppm NH_3

Figure 3 shows a long-time exposure of the sensor, showing that the resistance of the device drops back to its baseline when the desorption time is sufficiently long. Figure S2 shows the device response to changes in humidity; we see that a reduction (increase) in humidity leads to a reduction (increase) in device resistance. Figure S3 illustrates the combined effect of humidity and simultaneous ammonia exposure (as a result of using a bubbler as an ammonia source for that measurement).

Kelvin force probe microscopy[20] was used to determine the doping of the deposited film due to exposure to ammonia.

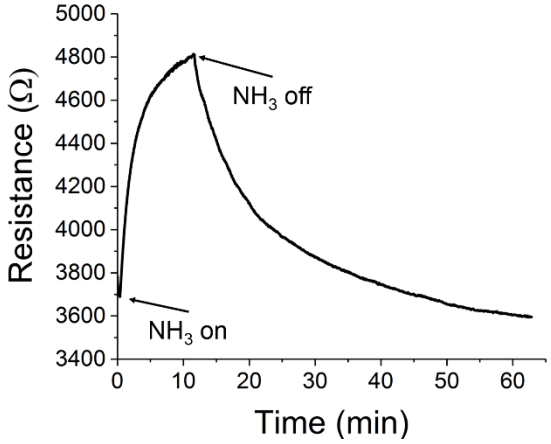

Figure 3 Exposure for 12 minutes to 150 ppm NH_3 and a desorption time of 45 minutes after which the device reaches its baseline

Figure 4a and 4b show the contact potential difference (CPD) before and after exposure to ammonia of the deposited film shown in Figure 4c. The shift is quantified in figure 4d with the histogram of both exposures.

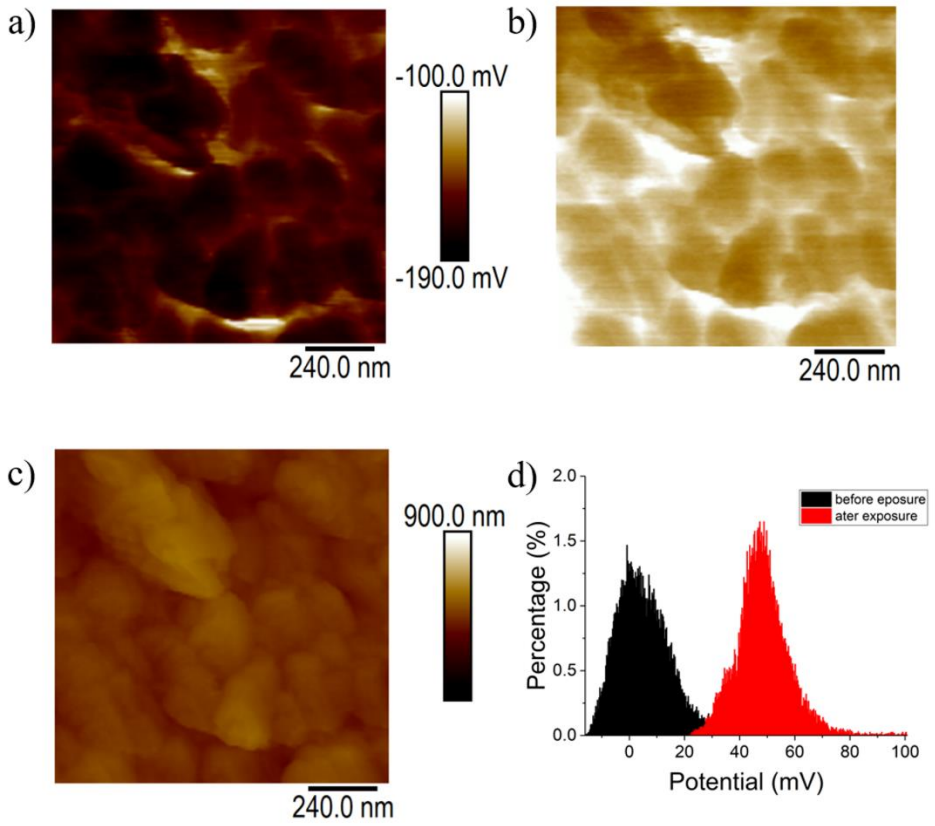

Figure 4 KPFM measurements of the surface CPD (a) before exposure and (b) after exposure to ammonia, (c) topography of measured percolating network using AFM, (d) pixel-wise histogram of surface CPD measurements, showing an approximately +50mV shift after ammonia exposure

The shift in CPD is around +50 meV showing the work function of the material is lowered. To confirm the doping Raman spectroscopy was used before and after the exposure to NH_3; see **Figure 5**. A shift in the D, G, 2D and G' features is visible due to doping; also the D' shoulder in the G peak has become more prominent. The shift in the G peak can be used to calculate the number of molecules adsorbed on the graphene[21] resulting in an estimate of ~$1.5x10^{12}$ cm^{-2}.

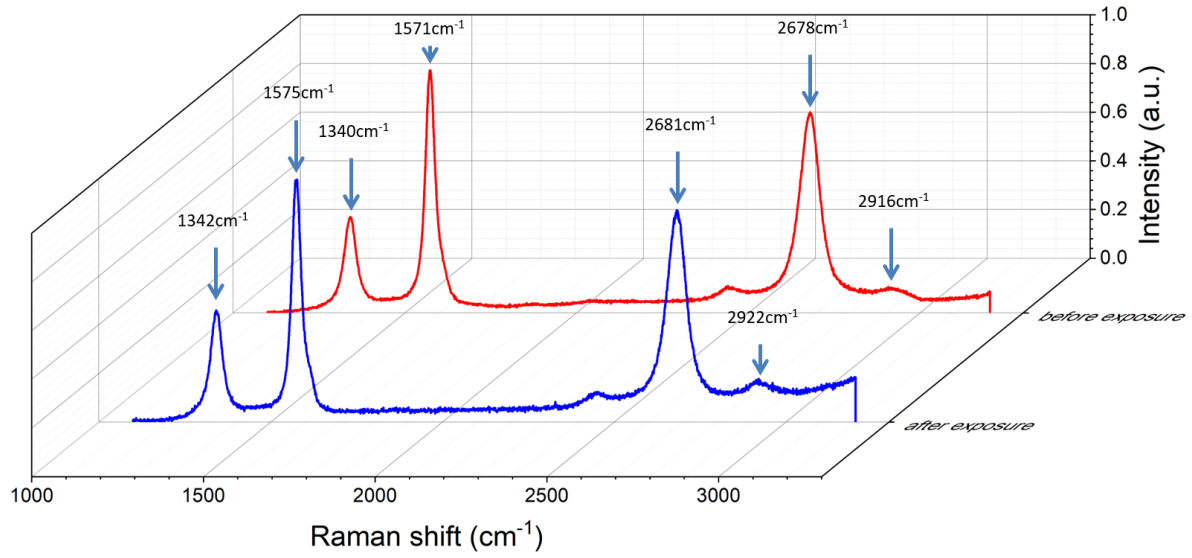

Figure 5 Raman spectrum before and after exposure to ammonia. Shifts in the D, G, 2D and G' peaks in positive direction are visible. The shifts correspond to doping of the graphene, the positive shift of the G and 2D peak indicates p-doping of the material and allows to calculate the number of adsorbed molecules[20] resulting in $1.5x10^{12}$ cm^{-2}

Comparing the potential shift from the KPFM analysis and the amount of molecules adsorbed with the dopant analysis of Das et al.[22] the shift of the potential for $1.5x10^{12}cm^{-2}$ adsorbed molecules is consistent with the 50 meV potential change measured. From the shift of the 2D peak in the positive direction n-doping is confirmed for ammonia exposure.[22]

Graphene at room temperature in a humid environment is naturally p-doped due to adsorbed water molecules.[23] NH_3 interacts predominantly with oxygen functionalities and defects in graphene and dopes the basal plane with electrons, thus reducing the number of majority carriers (holes) leading to an increase in sample resistance[24] as we have observed. This is confirmed by Kehayias et al.[25] who analysed a reduced graphene oxide (rGO) gas sensor in the same way.

These measurements do not confirm the sensing mechanism yet, as characteristically the conductivity in a percolating network is dominated by the contact resistance between individual particles rather than the bulk resistance of the material. In the case of carbon nanotubes the contact resistance is four orders of magnitude higher than the resistance of the tube itself,[26] therefore the contribution of the change in the resistance upon adsorption at the contacts needs to be considered as well.

First-principles studies have shown that the binding energy of NH_3 on graphene edge sites is six times higher than on the basal plane.[27,28] These values indicate the edge site adsorption is dominant over the basal plane adsorption, both of which contribute to the basal plane charge carrier density.

In order to understand the relative contributions of doping of the basal plan and inter-sheet resistance changes due to gas adsorption an identical measurement was performed using acetone which acts as an electron acceptor[29]. **Figure 6a** shows the KPFM analysis of the graphene nanosheets exposed to acetone, alongside a comparable resistance response (Figure 6b) to that shown in Figure 3.

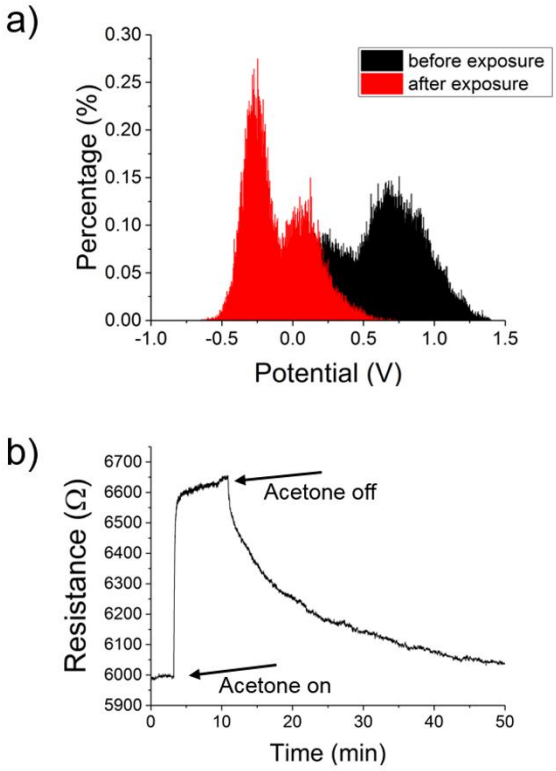

Figure 6 (a) Histogram of surface CPD before and after exposure to acetone, measured using KPFM. The peak at 0V originates from areas of the substrate which were not covered by nanosheets, and which do not shift with acetone exposure. (b) sensor resistance response to acetone exposure

The potential shift is in the opposite direction to that of the ammonia in Figure 4d. The device resistance in Figure 6b is seen to increase despite the increasing density of majority carriers (holes) due to depletion of electrons by the acetone. This indicates that the sensing mechanism is dominated by modification to the inter-sheet contact resistance rather than doping of the basal plane, as this would manifest as a decrease of resistance upon acetone exposure. The phenomenon of edge adsorption-dominated sensing response has been previously observed using dielectrophoresis of rGO which produces a similar

film structure to L-S deposition.[30]

The direction of the signal changes when exposed to dry air. Here a different sensing mechanism is taking place compared to the edge adsorption. It is well known that carbon materials at room temperature form a continuous layer of adsorbed water.[23] The conductivity of the material is strongly influenced by this water layer.[31] The mechanism of conduction is based on the Grotthuus chain reaction[32] (i.e. the transfer of a hydrogen atom between the water molecules[33]).

The binding energy of a molecule to the graphene can be inferred by exposing the system at different temperatures and fitting an exponential decay function, of the form $R = R_0 + \sum_i A_i \exp(-k_i t)$, to the desorption response using the least square method. The pre-exponential factors A_i dictate the relative contributions to the sensing response of the processes i each with a rate constant k_i. An example of this fitting to a single device exposure, using two exponential terms, is shown in **Figure 7a**. Figure 7b shows fitted rate constant k of the edge adsorption as a function of device temperature plotted as $1/\mathrm{k}_b T$, where k_b is the Boltzmann constant and T the absolute temperature.

The Arrhenius function $k(t) = A_0 \exp\left(\frac{-E_a}{k_b T}\right)$, where A_0 is a temperature-independent pre-factor, and E_a is interpreted as the binding energy of the contributions of the ammonia molecules to the graphene, is fitted to the measurements taken at different temperatures in Figure 7b.

The fitted value for the binding energy in this case is 100 meV. This is broadly consistent with theoretical predictions for the binding energy of ammonia molecules to the edge sites

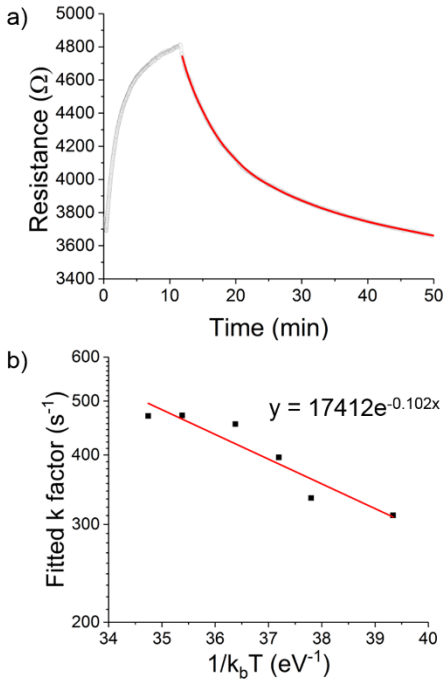

Figure 7 (a) Exponential fit to desorption of long term exposure to ammonia, (b) time constants at different temperatures with Arrhenius fit and corresponding equation

of graphene nanosheets.[27] This measurement confirms that edge-site binding is the dominant contribution to the chemiresistive response of these devices to ammonia exposure.

However, the desorption response is also influenced by the humidity in the measurement chamber which is not directly controlled in our experimental setup. This is due to the use of a bubbler as an ammonia source, which limits the accuracy of the binding energy measurement and makes the investigation of other processes more challenging. Nevertheless, this type of analysis is a promising method for understanding microscopic graphene-gas interactions using macroscopic, ensemble measurements.

3.Conclusion

We have demonstrated chemiresistive gas sensing by preparing devices using commercially available graphene and scalable production methodologies, such as L-S film deposition and laser electrode manufacturing. We have investigated a sensor structure consisting of percolating graphene platelets deposited using the L-S method. We confirm electronic doping of the basal plane using KPFM and Raman spectroscopy. Ammonia was found to n-dope the graphene whereas acetone was found to induce p-doping. The measured resistance of the system upon gas exposure to ammonia and acetone increases in both cases. We conclude from this that the inter-sheet resistance is responsible for the change in the resistance of the network rather than the intra-sheet conductivity. Fitting of the time-dependence of the desorption signal as a function of temperature is used to confirm that ammonia binding at edge sites is the dominant contribution to the overall device response. The binding energy obtained from Arrhenius analysis is consistent with predictions from the literature.

Such understanding of the sensing mechanism and response demonstrates the potential of these films both as a platform to study graphene-gas interactions and as low-cost scalable sensors.

4.Experimental Section

The substrates used were obtained from AimCore Technology (Hsinchu 30351, Taiwan); these consist of a glass substrate sputtered with molybdenum forming a 700 nm thick metallic layer. The graphene was obtained from Cambridge Nanosystems (Cambridge, UK) in a 1 mg mL^{-1} concentrated isopropanol (IPA) dispersion (G1 dispersion). An infrared nanosecond laser (Multiwave, set to 10ns, 1064 nm) and a Galvoscanner were used to pattern the IDEs into the metal. The laser was used in focus with a fluence of 3 J cm^{-2} at a mark speed of 1000 mm sec^{-1}. The finger electrode pattern was designed in a drawing interchange format (DXF) format created in a computer-aided design (CAD) to feed to the scanner. Graphene films were prepared as described by Fahimi et al.[17]. 2 mL of the graphene dispersion was spread onto the water sub-phase to form a Langmuir film at the air-water interface. The film was compressed from an initial area of 450 cm^2 at a rate of 30 cm^2 min^{-1} to a final area of 100 cm^2. The IDEs were lowered horizontally into contact with the sub-phase to transfer the compressed film to the device structure. Raman spectroscopy was performed using a Renishaw InVia microscope with a 532 nm solid-state laser, x20 objective, 10 second integration time and 5 mW power.

We setup a gas measurement system using a bubbler and dry air (schematic in supplementary information) to expose the devices to ammonia which was obtained in a 1 molar ammonium hydroxide solution from Sigma Aldrich. The pressure of the dry air

supply was held at 1 bar and the flow rate at 2 L min^{-1}. Diluted concentrations of ammonium hydroxide were put into the bubbler to reach different NH_3 concentrations in the measurement chamber. A reference sensor (a1-cbiss (Wirral, UK), GASBADGE PRO, Single Gas Detector, 1 ppm resolution) was used to measure the NH_3 concentration in the chamber. A temperature and humidity sensor was placed inside the chamber to ensure the measurement conditions remained constant. The devices were first exposed to ambient air with open lid and no dry air flow. The lid was closed and the flow regulated. For a short device exposure, the NH_3 concentration was measured after 2 min before the lid was opened to flush the device with ambient air. For a long exposure, the concentration was measured at 2 min and 15 min before the chamber was flushed. A Keithley 2420 and LabVIEW were used to measure the device resistance over time. A small ceramic hotplate was mechanically fixed to the back of the device for exposures at elevated temperatures.

Kelvin probe force microscopy was performed with a Bruker Dimension Icon atomic force microscope system using a platinum-iridium-coated silicon tip in peak force tapping mode using 5 nN contact force**.**

ASSOCIATED CONTENT

Supporting Information.

The Supporting Information is available free of charge on the ACS Publications website DOI:

Experimental setup, Humidity response

AUTHOR INFORMATION

Corresponding Author

*E-mail: Sebastian.nufer@m-solv.com

* E-mail: A.B.Dalton@sussex.ac.uk

Funding Sources

Marie Sklodowska-Curie grant agreement No 642742

ACKNOWLEDGMENT

We would like to thank Dimitrios Fantanas for useful discussions.

ABBREVIATIONS

CPD	Contact Potential Difference
IDE	Interdigitated Electrodes
KPFM	Kelvin Probe Force Microscopy
L-S	Langmuir-Schaefer

REFERENCES

(1) Zhang, Y.; Zhang, L.; Zhou, C. Review of Chemical Vapor Deposition of Graphene and Related Applications. *Accounts of chemical research* **2013**, *46*, 2329–2339.

(2) Shao, Y.; Wang, J.; Wu, H.; Liu, J.; Aksay, I. A.; Lin, Y. Graphene Based Electrochemical Sensors and Biosensors: A Review. *Electroanalysis* **2010**, *22*, 1027–

1036.

(3) Yuan, W.; Shi, G. Graphene-Based Gas Sensors. *Journal of Materials Chemistry A* **2013**, *1*, 10078–10091.

(4) Schedin, F.; Geim, A. K.; Morozov, S. V.; Hill, E. W.; Blake, P.; Katsnelson, M. I.; Novoselov, K. S. Detection of Individual Gas Molecules Adsorbed on Graphene. *Nat Mater* **2007**, *6*, 652–655.

(5) Chen, G.; Paronyan, T. M.; Harutyunyan, A. R. Sub-Ppt Gas Detection with Pristine Graphene. *Applied Physics Letters* **2012**, *101*, 053119.

(6) Lu, G.; Park, S.; Yu, K.; Ruoff, R. S.; Ocola, L. E.; Rosenmann, D.; Chen, J. Toward Practical Gas Sensing with Highly Reduced Graphene Oxide: A New Signal Processing Method to Circumvent Run-to-Run and Device-to-Device Variations. *ACS nano* **2011**, *5*, 1154–1164.

(7) Lipatov, A.; Varezhnikov, A.; Wilson, P.; Sysoev, V.; Kolmakov, A.; Sinitskii, A. Highly Selective Gas Sensor Arrays Based on Thermally Reduced Graphene Oxide. *Nanoscale* **2013**, *5*, 5426–5434.

(8) Some, S.; Xu, Y.; Kim, Y.; Yoon, Y.; Qin, H.; Kulkarni, A.; Kim, T.; Lee, H. Highly Sensitive and Selective Gas Sensor Using Hydrophilic and Hydrophobic Graphenes. *Scientific reports* **2013**, *3*, 1868.

(9) Zhou, L.; Shen, F.; Tian, X.; Wang, D.; Zhang, T.; Chen, W. Stable Cu 2 O Nanocrystals Grown on Functionalized Graphene Sheets and Room Temperature H 2 S Gas Sensing with Ultrahigh Sensitivity. *Nanoscale* **2013**, *5*, 1564–1569.

(10) Ko, G.; Kim, H.-Y.; Ahn, J.; Park, Y.-M.; Lee, K.-Y.; Kim, J. Graphene-Based Nitrogen Dioxide Gas Sensors. *Current Applied Physics* **2010**, *10*, 1002–1004.

(11) Rumyantsev, S.; Liu, G.; Shur, M. S.; Potyrailo, R. A.; Balandin, A. A. Selective Gas Sensing with a Single Pristine Graphene Transistor. *arXiv preprint arXiv:1204.5238* **2012**.

(12) Tran, Q. T.; Huynh, T. M. H.; Tong, D. T.; Nguyen, N. D.; others. Synthesis and Application of Graphene-Silver Nanowires Composite for Ammonia Gas Sensing. *Advances in Natural Sciences: Nanoscience and Nanotechnology* **2013**, *4*, 045012.

(13) Avouris, P.; Dimitrakopoulos, C. Graphene: Synthesis and Applications. *Materials Today* **2012**, *15*, 86–97.

(14) Yu, K.; Bo, Z.; Lu, G.; Mao, S.; Cui, S.; Zhu, Y.; Chen, X.; Ruoff, R. S.; Chen, J. Growth of Carbon Nanowalls at Atmospheric Pressure for One-Step Gas Sensor Fabrication. *Nanoscale Res Lett* **2011**, *6*, 202.

(15) Shirk, M.; Molian, P. A Review of Ultrashort Pulsed Laser Ablation of Materials. *Journal of Laser Applications* **1998**, *10*, 18–28.

(16) Gengler, R. Y.; Veligura, A.; Enotiadis, A.; Diamanti, E. K.; Gournis, D.; Józsa, C.; van Wees, B. J.; Rudolf, P. Large-Yield Preparation of High-Electronic-Quality Graphene by a Langmuir-Schaefer Approach. *small* **2010**, *6*, 35–39.

(17) Fahimi, A.; Jurewicz, I.; Smith, R. J.; Sharrock, C. S.; Bradley, D. A.; Henley, S. J.; Coleman, J. N.; Dalton, A. B. Density Controlled Conductivity of Pristine Graphene Films. *Carbon* **2013**, *64*, 435–443.

(18) Kostiuk, D.; Luby, S.; Demydenko, M.; Jergel, M.; Siffalovic, P.; Ivanco, J.; Majkova, E. Few-Layer Graphene Langmuir-Schaefer Nanofilms for H 2 Gas Sensing. *Procedia Engineering* **2016**, *168*, 243–246.

(19) Rao, F.; Almumen, H.; Fan, Z.; Li, W.; Dong, L. Inter-Sheet-Effect-Inspired Graphene Sensors: Design, Fabrication and Characterization. *Nanotechnology* **2012**, *23*, 105501.

(20) Melitz, W.; Shen, J.; Kummel, A. C.; Lee, S. Kelvin Probe Force Microscopy and Its Application. *Surface Science Reports* **2011**, *66*, 1–27.

(21) Kim, S.; Park, S.; Kim, H.; Jang, G.; Park, D.; Park, J.-Y.; Lee, S.; Ahn, Y. Characterization of Chemical Doping of Graphene by in-Situ Raman Spectroscopy. *Applied Physics Letters* **2016**, *108*, 203111.

(22) Das, A.; Pisana, S.; Chakraborty, B.; Piscanec, S.; Saha, S.; Waghmare, U.; Novoselov, K.; Krishnamurthy, H.; Geim, A.; Ferrari, A. Monitoring Dopants by Raman Scattering in an Electrochemically Top-Gated Graphene Transistor. *Nature nanotechnology* **2008**, *3*, 210–215.

(23) Pinto, H.; Markevich, A. Electronic and Electrochemical Doping of Graphene by Surface Adsorbates. *Beilstein journal of nanotechnology* **2014**, *5*, 1842–1848.

(24) Gautam, M.; Jayatissa, A. H. Ammonia Gas Sensing Behavior of Graphene Surface Decorated with Gold Nanoparticles. *Solid-State Electronics* **2012**, *78*, 159–165.

(25) Kehayias, C. E.; MacNaughton, S.; Sonkusale, S.; Staii, C. Kelvin Probe Microscopy and Electronic Transport Measurements in Reduced Graphene Oxide Chemical Sensors. *Nanotechnology* **2013**, *24*, 245502.

(26) Hu, L.; Hecht, D.; Grüner, G. Percolation in Transparent and Conducting Carbon Nanotube Networks. *Nano letters* **2004**, *4*, 2513–2517.

(27) Huang, B.; Li, Z.; Liu, Z.; Zhou, G.; Hao, S.; Wu, J.; Gu, B.-L.; Duan, W. Adsorption of Gas Molecules on Graphene Nanoribbons and Its Implication for Nanoscale Molecule

Sensor. *The Journal of Physical Chemistry C* **2008**, *112*, 13442–13446.

(28) Leenaerts, O.; Partoens, B.; Peeters, F. Adsorption of H 2 O, N H 3, CO, N O 2, and NO on Graphene: A First-Principles Study. *Physical Review B* **2008**, *77*, 125416.

(29) Snow, E. S.; Perkins, F. K. Capacitance and Conductance of Single-Walled Carbon Nanotubes in the Presence of Chemical Vapors. *Nano Letters* **2005**, *5*, 2414–2417.

(30) MacNaughton, S.; Sonkusale, S.; Surwade, S.; Ammu, S.; Manohar, S. Carbon Nanotube and Graphene Based Gas Micro-Sensors Fabricated by Dielectrophoresis on Silicon. In *Sensors, 2010 IEEE*; 2010; pp. 894–897.

(31) Nufer, S.; Fantanas, D.; Ogilvie, S. P.; Large, M. J.; Winterauer, D.; Salvage, J. P.; Meloni, M.; King, A. A.; Schellenberger, P.; Shmeliov, A. Percolating Metallic Structures Templated on Laser-Deposited Carbon Nanofoams Derived from Graphene Oxide: Applications in Humidity Sensing. *ACS Applied Nano Materials* **2018**.

(32) Ernsberger, F. M. The Nonconformist Ion. *Journal of the American Ceramic Society* **1983**, *66*, 747–750.

(33) Lin, W.-D.; Chang, H.-M.; Wu, R.-J. Applied Novel Sensing Material Graphene/polypyrrole for Humidity Sensor. *Sensors and Actuators B: Chemical* **2013**, *181*, 326–331.

TOC – Figure

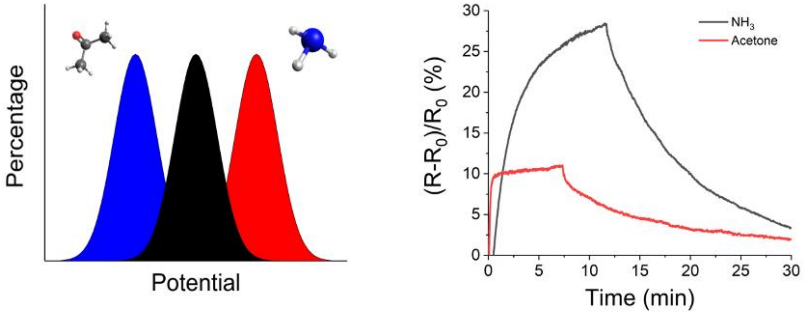

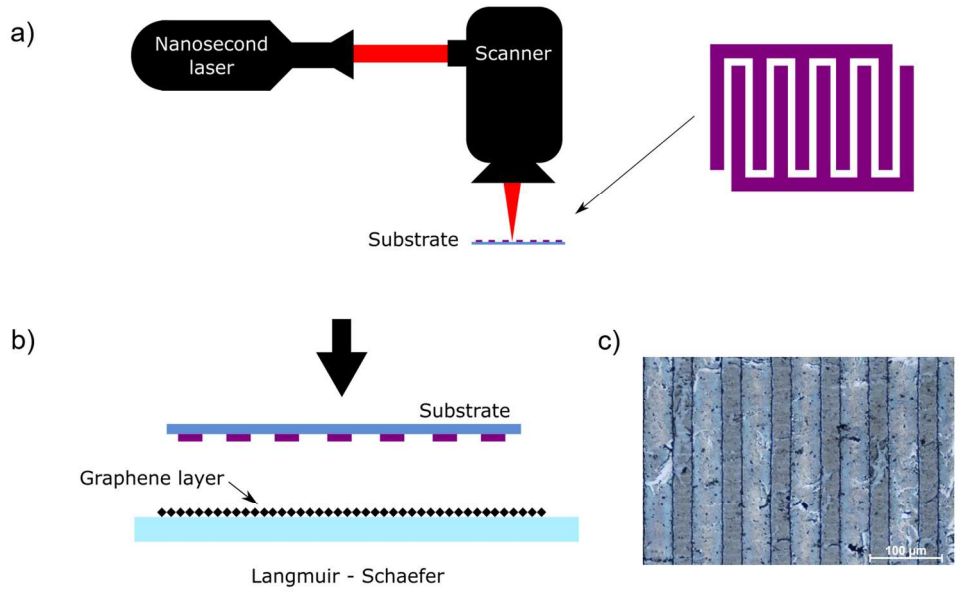

Figure 1 (a) Experimental laser setup used to ablate interdigitated electrodes into a metallic substrate. An infrared nanosecond laser is guided into a Galvoscanner which scribes the designed pattern into the substrate, (b) Langmuir – Schaefer was used to directly deposit graphene on to the IDEs, (c) optical micrograph of the fabricated device

170x104mm (300 x 300 DPI)

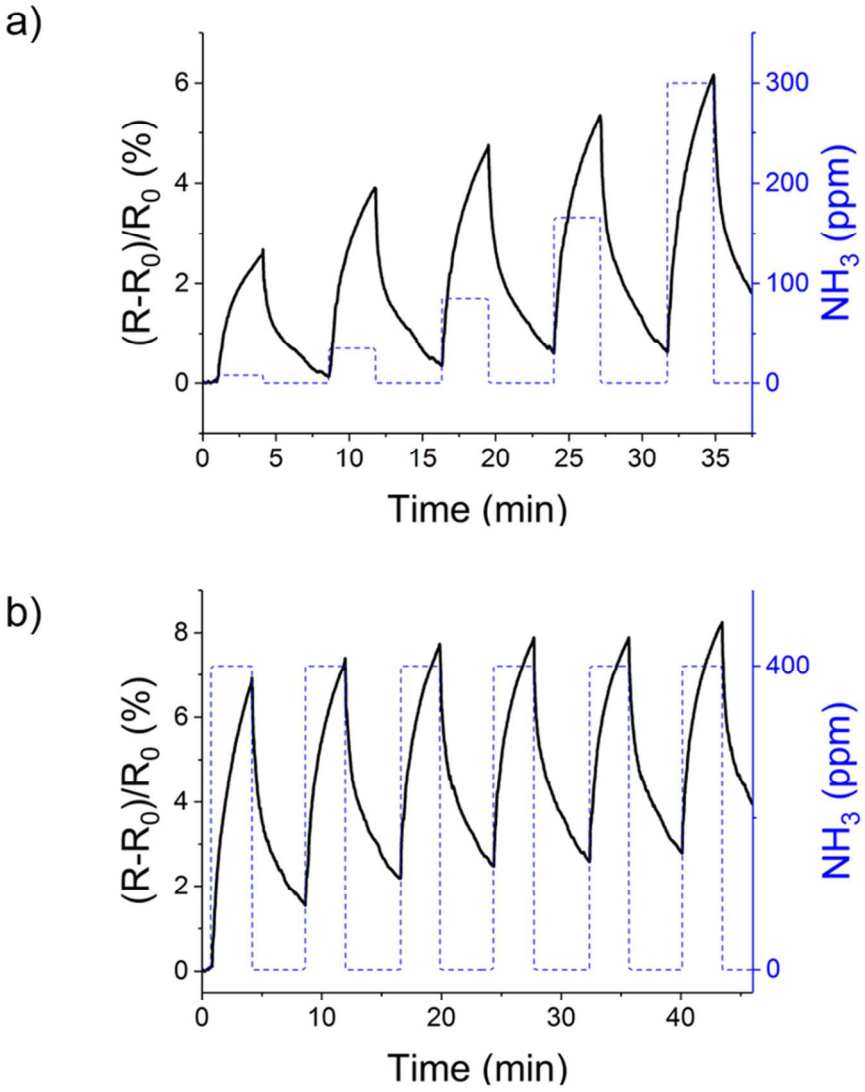

Figure 2 (a) relative signal to various concentrations of NH_3, (b) relative signal to a repeated concentration of 400 ppm NH_3

80x104mm (300 x 300 DPI)

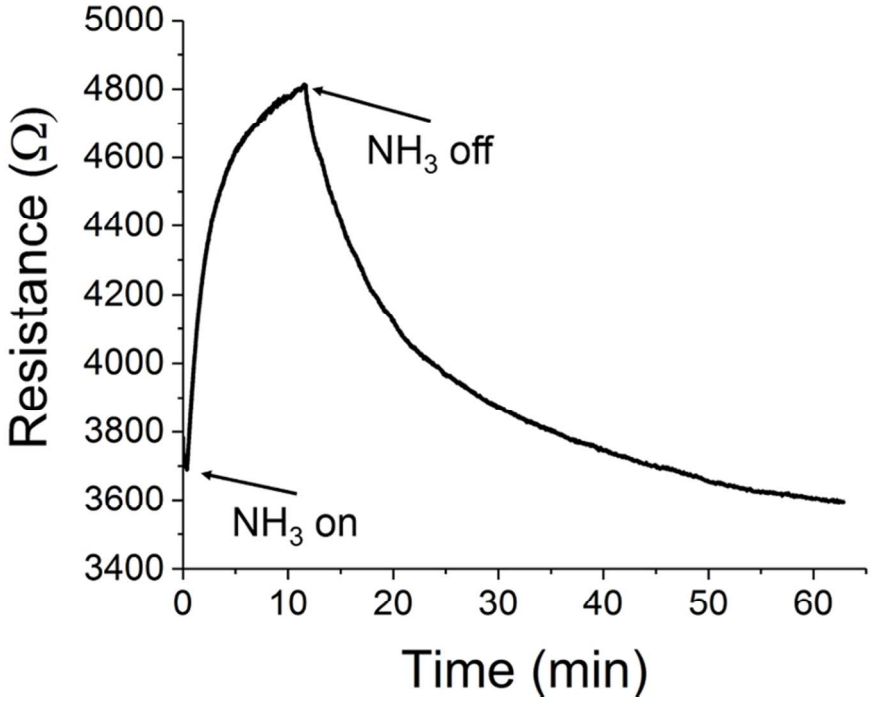

Figure 3 Exposure for 12 minutes to 150 ppm NH_3 and a desorption time of 45 minutes after which the device reaches its baseline

80x61mm (300 x 300 DPI)

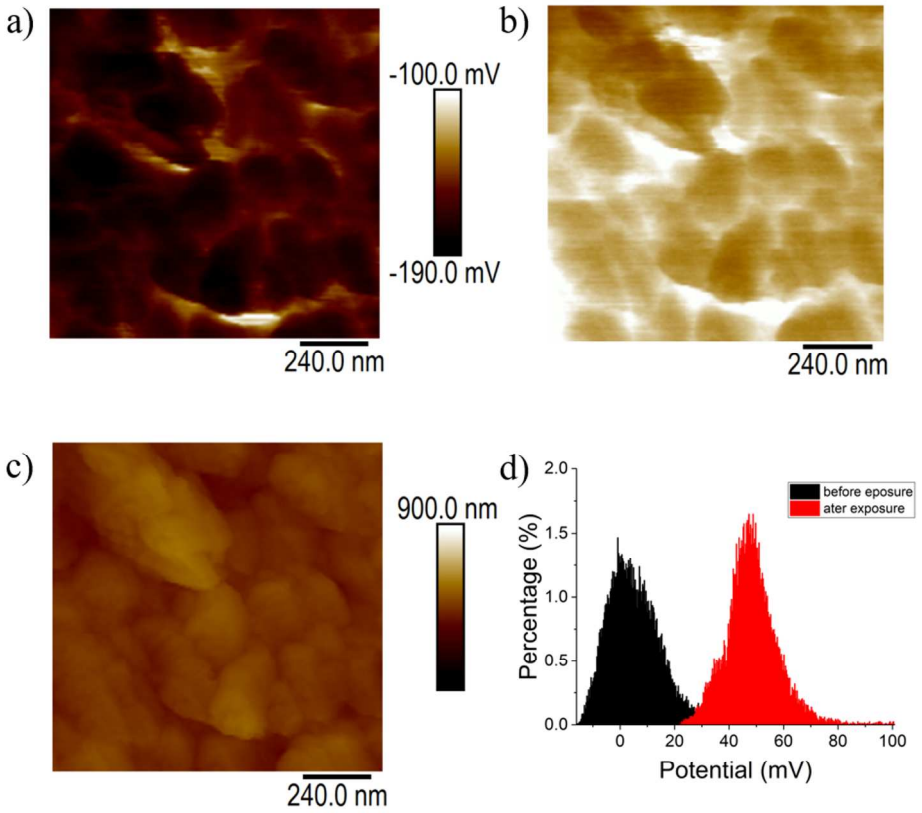

Figure 4 KPFM measurements of the surface CPD (a) before exposure and (b) after exposure to ammonia, (c) topography of measured percolating network using AFM, (d) pixel-wise histogram of surface CPD measurements, showing an approximately +50mV shift after ammonia exposure

175x160mm (300 x 300 DPI)

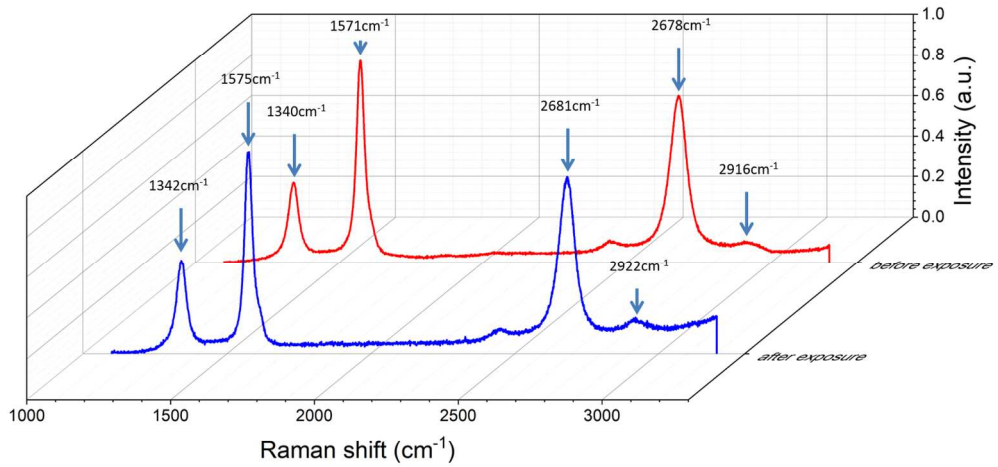

Figure 5 Raman spectrum before and after exposure to ammonia. Shifts in the D, G, 2D and G' peaks in positive direction are visible. The shifts correspond to doping of the graphene, the positive shift of the G and 2D peak indicates p-doping of the material and allows to calculate the number of adsorbed molecules20 resulting in 1.5.x1012 cm^{-2}

170x88mm (300 x 300 DPI)

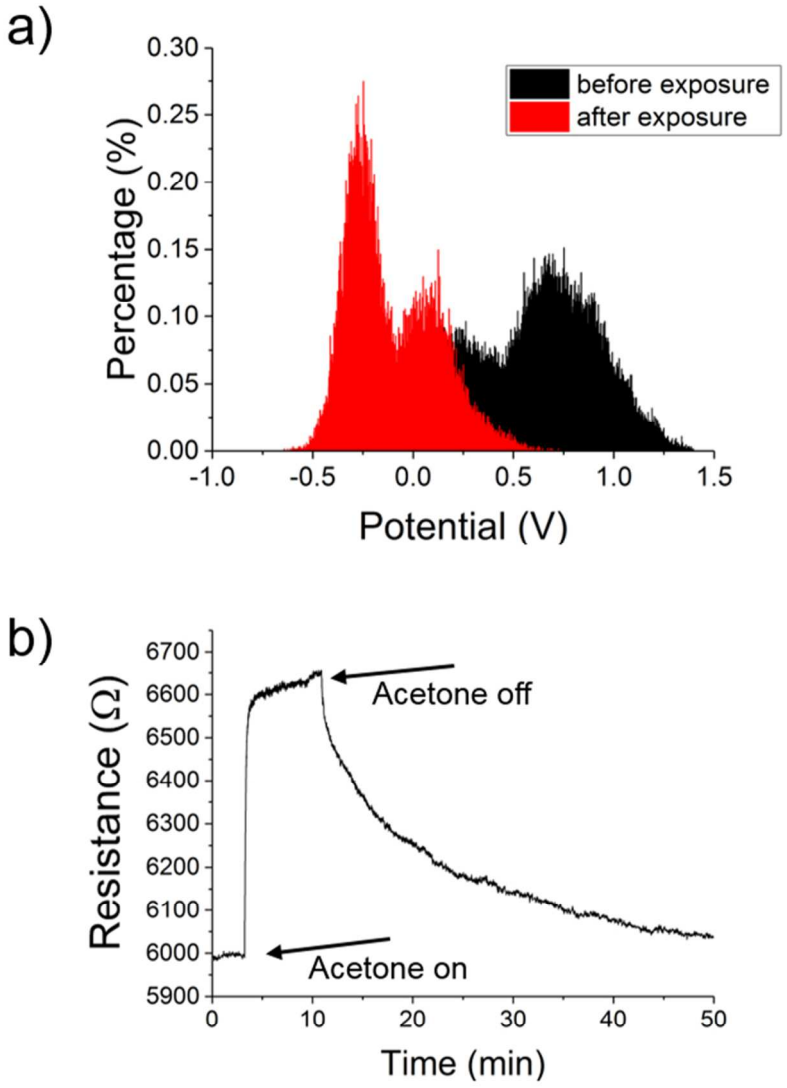

Figure 6 (a) Histogram of surface CPD before and after exposure to acetone, measured using KPFM. The peak at 0V originates from areas of the substrate which were not covered by nanosheets, and which do not shift with acetone exposure. (b) sensor resistance response to acetone exposure

80x108mm (300 x 300 DPI)

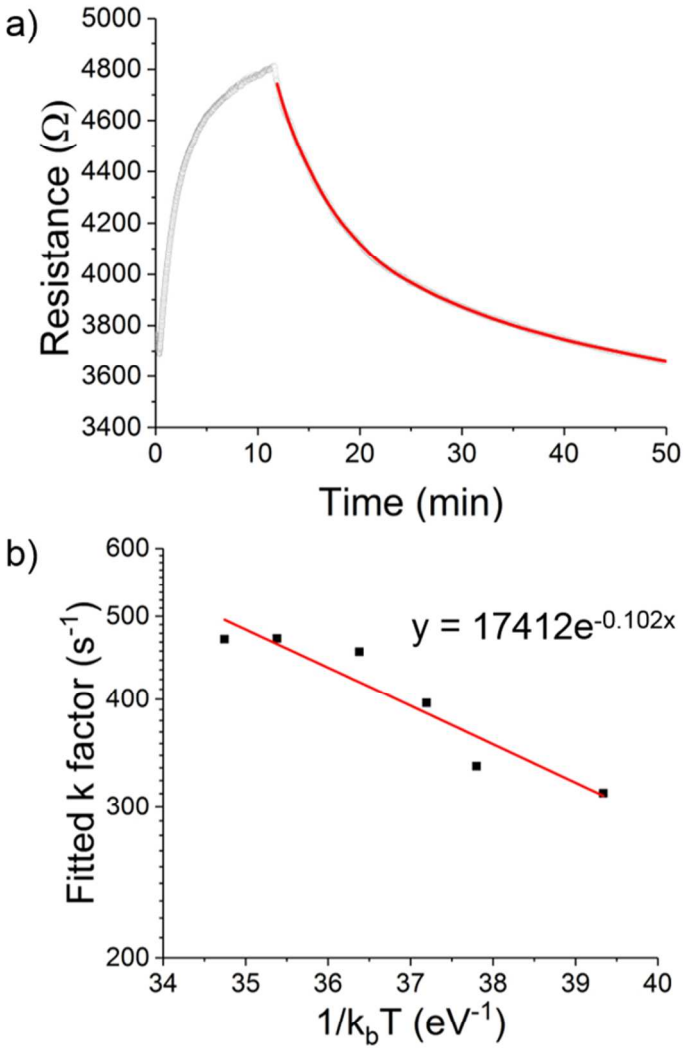

Figure 7 (a) Exponential fit to desorption of long term exposure to ammonia, (b) time constants at different temperatures with Arrhenius fit and corresponding equation

80x98mm (300 x 300 DPI)